

UAV Communications in Integrated Terrestrial and Non-terrestrial Networks

Mohamed Benzaghta^{*}, Giovanni Geraci^{*}, Rasoul Nikbakht^b, and David López-Pérez[#]

^{*}Universitat Pompeu Fabra (UPF), Barcelona, Spain

^bCentre Tecnològic de Telecomunicacions de Catalunya (CTTC), Barcelona, Spain

[#]Huawei Technologies, Boulogne-Billancourt, France

Abstract—With growing interest in integrating terrestrial networks (TNs) and non-terrestrial networks (NTNs) to connect the unconnected, a key question is whether this new paradigm could also be opportunistically exploited to augment service in urban areas. We assess this possibility in the context of an integrated TN-NTN, comprising a ground cellular deployment paired with a Low Earth Orbit (LEO) satellite constellation, providing sub-6 GHz connectivity to an urban area populated by ground users (GUEs) and uncrewed aerial vehicles (UAVs). Our study reveals that offloading UAV traffic to the NTN segment drastically reduces the downlink outage of UAVs from 70% to nearly zero, also boosting their uplink signal quality as long as the LEO satellite constellation is sufficiently dense to guarantee a minimum elevation angle. Offloading UAVs to the NTN also benefits coexisting GUEs, preventing uplink outages of around 12% that GUEs would otherwise incur. Despite the limited bandwidth available below 6 GHz, NTN-offloaded UAVs meet command and control rate requirements even across an area the size of Barcelona with as many as one active UAV per cell. Smaller UAV populations yield proportionally higher rates, potentially enabling aerial broadband applications.

I. INTRODUCTION

Thanks to their low cost and high mobility, uncrewed aerial vehicles (UAVs) may soon take over important tasks including search and rescue, delivery, and remote sensing. In the next decade, UAV taxis may also redefine how we commute and, in turn, where we live and work. For these and other applications, UAVs will transfer real-time data to and from the mobile network, requiring reliable connectivity for command and control (C&C) and mission-specific data payloads [1]–[7].

Due to their height, however, UAVs receive/create line-of-sight (LoS) interfering signals from/to a plurality of cells, respectively hindering the decoding of C&C messages and disrupting the service of legacy ground users (GUEs) [8]–[10]. Technical solutions to this problem have been introduced in 4G LTE [11] and 5G NR [12] to deal with a handful of connected UAVs. More advanced solutions hinge, e.g., on uptilted cells [13]–[15], massive MIMO [16], or cell-free architectures [17], and may be less economically viable in the short term, as they necessitate dedicated network upgrades.

As an alternative to ground densification, UAVs could be supported by non-terrestrial networks (NTNs), e.g., via Low

Earth Orbit (LEO) satellite constellations [18]–[21]. While mainly targeting underserved areas, NTNs may also be leveraged to augment urban connectivity, e.g., with a terrestrial network (TN) operator opportunistically leasing spectrum and infrastructure from an NTN one. Indeed, the ongoing 3GPP efforts towards TN-NTN integration will allow mobile devices to seamlessly switch from one segment to the other [22]–[24].

In this paper, we consider an integrated TN-NTN, comprising a ground cellular deployment paired with a LEO satellite constellation, providing sub-6 GHz connectivity to an urban area populated by ground users (GUEs) and UAVs. We study the benefits of offloading the latter to the NTN, both in the downlink (DL) and uplink (UL), for different satellite elevation angles and beam reuse schemes, while also accounting for the main propagation features, antenna models, and deployment scenarios specified by the 3GPP. Our main findings can be summarized as follows:

- UAVs connected to a standalone TN incur a nearly 70% downlink outage when flying at 150m due to ground-to-air interference. Offloading UAV traffic to the NTN segment ensures reliable coverage, also outperforming a TN that implements interference coordination.
- TN-connected UAVs generate strong uplink interference, forcing—in the most challenging scenario—up to 12% of the GUEs into outage, even under practical fractional power control. Such outage is reduced to below 1% when UAV uplink traffic is offloaded to the NTN.
- Under inter-beam interference, NTN-offloaded UAVs may experience outage when the NTN elevation angle falls to 87° and below, calling for a careful design of beam reuse according to the LEO constellation density.
- For an area the size of Barcelona, the NTN can provide C&C rates of 60-100 kbps for as many as one UAV per TN cell. Lower UAV penetration yields proportionally higher rates, potentially enabling broadband use-cases.

II. SYSTEM MODEL

In this section, we introduce the network topology and channel models used. Further details are given in Table I.

A. Integrated TN-NTN Deployment

We consider a cellular TN as specified by 3GPP [11], [25]. We also assume the availability of an NTN segment through

M. Benzaghta and G. Geraci were in part supported by MINECO's Project RTI2018-101040 and by a "Ramón y Cajal" Fellowship. Part of the work of R. Nikbakht was carried out while he was with Universitat Pompeu Fabra.

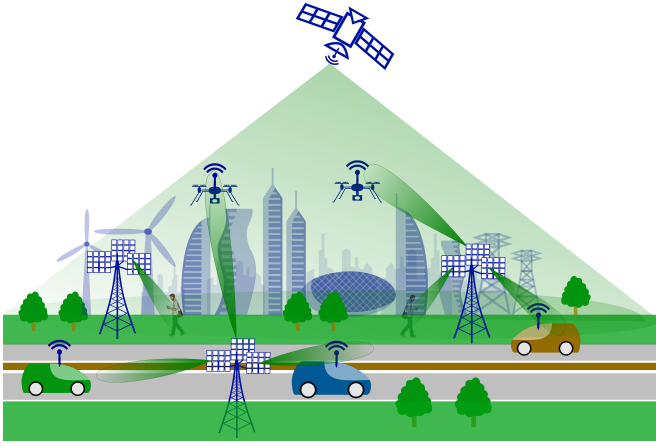


Fig. 1: Illustration of an integrated TN-NTN comprising a terrestrial and a satellite segment serving GUEs and UAVs in an urban area.

a LEO satellite orbiting at 600 km, whose features are chosen according to [23], [24].¹ We consider handheld GUEs and UAVs, all capable of connecting to either the TN or NTN.

Terrestrial network: Base stations (BSs) are deployed on a hexagonal layout, and communicate with their respective sets of connected users in downlink and uplink. Deployment sites are comprised of three co-located BSs, each covering one sector—i.e., a TN cell—spanning an angular interval of 120° . For an inter-site distance ISD_{TN} , the area of a TN cell is given by $A_{TN} = \sqrt{3} \cdot ISD_{TN}^2 / 6$.

Non-terrestrial network: The LEO satellite segment generates multiple beams to serve users in both downlink and uplink. The beams point to the ground in a hexagonal fashion, each creating one corresponding NTN cell. The spacing between adjacent beams is computed according to the half-power beamwidth (HPBW) of each beam’s radiation pattern. Due to its orbital movement, the LEO satellite is seen under different elevation angles from the standpoint of the TN, and accordingly, the footprint of its Earth-moving beams illuminates different areas on the ground. We study how the NTN performance is affected by the elevation angle, since this has implications on the LEO constellation density needed.

User population: Both the TN and NTN are capable of serving GUEs and UAVs, e.g., providing the former with data and the latter with data and C&C information. We assume the total user population to be concentrated in an urban area of size A_U , contained in an NTN cell and resulting in a total of A_U/A_{TN} TN cells. In this area, GUEs are located both outdoor, at height $h_{out} = 1.5$ m, and indoor, at h_{in} in buildings consisting of several floors. UAVs fly outdoor at height h_{UAV} .

Spectrum allocation: We assume the TN and NTN to employ orthogonal bands and frequency division duplexing (FDD). For both the TN and NTN, we assume the nominal downlink and uplink carrier frequencies to be at 2 GHz [23].

¹As the penetration of UAVs increases, a TN operator intending to provide aerial connectivity may choose to lease infrastructure and spectrum from an NTN operator [22]. While the latter would primarily deploy and operate LEO constellations to cover currently underserved areas, their inherent mobility makes them available over urban areas as well, generating opportunities in the multi-operator scenario considered in this paper.

For the TN, the available bandwidth is fully reused across all cells. For the NTN, we consider two possible frequency reuse factors (FRF), namely: (i) $FRF = 1$, where all frequency resources are fully reused across all beams, and (ii) $FRF = 3$, where they are partitioned into three sets, each reused every three beams. As it will be shown, the latter approach sacrifices peak performance in favor of reducing interference between adjacent beams and in turn enhance cell-edge performance.

B. Propagation Channel

The main propagation channel features are described in the following and summarized in Table I.

Path loss and shadow fading: All radio links are affected by path loss and lognormal shadow fading, both dependent on the link LoS condition, and modeled as in [11], [24]. TN links explicitly account for the transmitter and receiver heights, as this is crucial when modeling cellular-connected UAV users, with higher UAVs more likely to experience LoS condition from a plurality of cells [11]. NTN links account for the LEO satellite elevation angle, i.e., the angle between the line pointing towards the satellite and the local horizontal plane. Elevation angles closer to nadir, i.e., 90° , yield shorter LEO-to-user distances and are more likely to be in LoS [24]. Compared to a TN link, the signal travelling on an NTN link undergoes several extra stages of propagation. As a result, the total path loss consists of additional terms accounting for the attenuation due to atmospheric gases and to scintillation.

Antenna gain: We assume all GUEs and UAVs to have a single omnidirectional antenna with unitary gain. We assume each TN BS to be equipped with a vertical, downtilted, uniform linear array, with semi-directive elements and a single radio-frequency chain. The latter yields a realistic radiation pattern, modeling the upper sidelobes seen by UAVs [26]. Lastly, we assume the antenna generating each LEO satellite beam to be a typical reflector with circular aperture [24].

The total large-scale power gain on a link comprises path loss, shadow fading, and antenna gain at both transmitter and receiver. We denote $G_{x,k}$ the large-scale power gain between cell x and user k , with the subscript $x \in \{t, n\}$ referring either to a specific TN cell t or a specific NTN cell n .

Small-scale fading: Similarly, we denote $h_{x,k}$ the small-scale block fading between cell x and user k . We assume TN-connected GUEs to undergo Rayleigh fading and UAV links to experience pure LoS propagation conditions, given their elevated position with respect to the clutter of buildings.²

Power control (TN): In the downlink, we assume all TN BSs to transmit the same power P_t . In the uplink, we consider open-loop fractional power control for all users connected to the TN, as per the cellular systems currently deployed. Accordingly, the power P_k transmitted by a given user k is adjusted depending on the serving TN cell t as [27]

$$P_k = \min \{ P^{\max}, P_0 \cdot G_{t,k}^\alpha \}, \quad (1)$$

²Different small-scale fading assumptions only yield anecdotal quantitative changes in the numerical results presented. They could however play a more prominent role when considering spatial multiplexing and antenna correlation.

TABLE I: System parameters

TN deployment	
Cell layout	Hexagonal grid over an area $A_U = 52 \text{ km}^2$, $\text{ISD}_{\text{TN}} = 500 \text{ m}$, three sectors per site, one BS per sector at 25 m [11]
Frequency band	FRF=1, $B_x = 10+10 \text{ MHz}$ (DL+UL) at 2 GHz [11]
BS transmit power	46 dBm [11]
Antenna elements	Horiz./vert. HPBW: 65° , max. gain: 8 dBi [11]
Antenna array	10×1 , downtilt: 12° , element spacing: 0.5λ [11]
Noise figure	7 dB [25]
NTN deployment	
Cell layout	Orbit: 600 km, 7 beams centered on a hexagonal grid, elevation angle: variable [23]
Frequency band	FRF=1, $B_x = 30+30 \text{ MHz}$ (DL+UL) at 2 GHz [23] FRF=3, $B_x = 10+10 \text{ MHz}$ (DL+UL) at 2 GHz [23]
Transmit power	34 dBW/MHz per beam [23]
Beam antenna	Reflector with circular aperture, HPBW: 4.41° , max. gain: 30 dBi [23]
G/T	1.1 dB/K antenna gain-to-noise-temperature [23]
Users	
User distribution	15 users per TN sector on average [11]
GUE distribution	80% indoor, horiz.: uniform, h_{in} : uniform in buildings of four to eight floors [25]
	20% outdoor, horiz.: uniform, $h_{\text{out}} = 1.5 \text{ m}$ [25]
UAV distribution	Outdoor, horiz.: uniform, $h_{\text{UAV}}: 150 \text{ m}$ [11]
UAVs/GUEs ratio	3GPP Case 2: 0.7%, Case 3: 7.1% [11]
User association	Based on RSRP (large-scale fading)
Scheduler	DL: single-user round robin, $B_k = B_x$
	UL: multi-user round robin, $B_k = 360 \text{ kHz}$ [18]
UL power control	TN: fractional power control with $\alpha = 0.80$, $P_0 = -85 \text{ dBm}$, and $P_{\text{max}} = 23 \text{ dBm}$ [11]
	NTN: always max power $P_{\text{max}} = 23 \text{ dBm}$ [23]
User antenna	Omnidirectional, gain: 0 dBi [11]
Noise figure	9 dB [11]
Channel model	
Large-scale fading	Urban Macro as per [11], [24], [25]
Small-scale fading	TN-GUE: Rayleigh
	TN-UAV and NTN-UAV: pure LoS
Thermal noise	-174 dBm/Hz spectral density [11]

where P^{max} is the user's maximum transmit power, P_0 is a parameter adjusted by the network, the exponent $\alpha \in [0, 1]$ is the fractional power control factor, and $G_{t,k}$ is the large-scale fading between user k and TN cell t . The aim of (1) is to compensate for a fraction α of the large-scale fading, up to a limit imposed by P^{max} .

Power control (NTN): Uplink fractional power control is not applied to users connected to the NTN, with the latter transmitting at maximum power $P_k = P^{\text{max}}$. Similarly, a fixed downlink power P_n is always used by each NTN cell [23].

III. EVALUATION METHODOLOGY

To study the gains provided by a NTN segment, we compare the performance of GUEs and UAVs in an integrated TN-NTN to the one experienced in a baseline standalone TN. In this section, we introduce the association and user offloading policy adopted in each case. Furthermore, we elaborate on the key performance indicators of interest.

A. Cell Association and User Offloading

We denote as \mathcal{T} and \mathcal{N} the sets of TN and NTN cells, respectively, and as \mathcal{U}_x the set of active users associated to cell x . We denote \mathcal{S}_T and \mathcal{S}_N as the set of users served by the TN and NTN, respectively.

Standalone TN: In the conventional case of a standalone TN, all GUEs and UAVs associate to the TN cell providing the largest reference signal received power (RSRP). For user k , the latter corresponds to the cell x providing the highest large-scale gain $G_{x,k}$.

UAV offloading to the NTN: In the case of an integrated TN-NTN, we assume all GUEs to be served by the TN and UAV users to be offloaded to the NTN segment.³ As it will be clear in the numerical results section, this choice is triggered by the mutual interference between aerial and ground transmissions, where the performance of UAVs (resp. GUEs) can be severely impaired in the downlink (resp. uplink) [16].

B. Key Performance Indicators

Under the orthogonal spectrum allocation between TN and NTN, the DL and UL signal-to-interference-plus-noise ratios (SINRs) on a given time-frequency physical resource block (PRB) of user k served by TN cell t are respectively given by

$$\text{SINR}_{t,k}^{\text{DL}} = \frac{P_t \cdot G_{t,k} \cdot |h_{t,k}|^2}{\sum_{\tau \in \mathcal{T} \setminus t} P_\tau \cdot G_{\tau,k} \cdot |h_{\tau,k}|^2 + \sigma_k^2}, \quad (2)$$

$$\text{SINR}_{t,k}^{\text{UL}} = \frac{P_k \cdot G_{t,k} \cdot |h_{t,k}|^2}{\sum_{\ell \in \mathcal{S}_T \setminus k} P_\ell \cdot G_{t,\ell} \cdot |h_{t,\ell}|^2 + \sigma_k^2}, \quad (3)$$

where σ_k^2 is the thermal noise variance over the bandwidth B_k accessed by user k . Similarly, the DL and UL SINRs per PRB of user k served by NTN cell n are respectively given by

$$\text{SINR}_{n,k}^{\text{DL}} = \frac{P_n \cdot G_{n,k} \cdot |h_{n,k}|^2}{\sum_{\nu \in \mathcal{N} \setminus n} P_\nu \cdot G_{\nu,k} \cdot |h_{\nu,k}|^2 + \sigma_k^2}, \quad (4)$$

$$\text{SINR}_{n,k}^{\text{UL}} = \frac{P_k \cdot G_{n,k} \cdot |h_{n,k}|^2}{\sum_{\ell \in \mathcal{S}_N \setminus k} P_\ell \cdot G_{n,\ell} \cdot |h_{n,\ell}|^2 + \sigma_k^2}. \quad (5)$$

The rate \mathcal{R}_k achievable by user k served by cell x can be related to its SINR (either in downlink or uplink) as

$$\mathcal{R}_k = \eta_k B_k \mathbb{E}[\log_2(1 + \text{SINR}_{x,k})], \quad (6)$$

with x denoting the serving TN or NTN cell depending on the user's association, B_k the bandwidth allocated to user k , and η_k the fraction of time user k is scheduled by cell x , and where the expectation is taken over the small-scale fading. In the downlink, we assume each cell x to multiplex its set of associated users \mathcal{U}_x in the time domain, yielding $\eta_k = |\mathcal{U}_x|^{-1}$, and to allocate the entire available band B_x to the scheduled user k , i.e., $B_k = B_x$. In the uplink, we assume user multiplexing to occur both in the time and frequency domains, with each user allocated a bandwidth B_k and $N_x =$

³The study of a case-by-case offloading policy, accounting for factors such as the UAV height and the cell load will be the subject of future work.

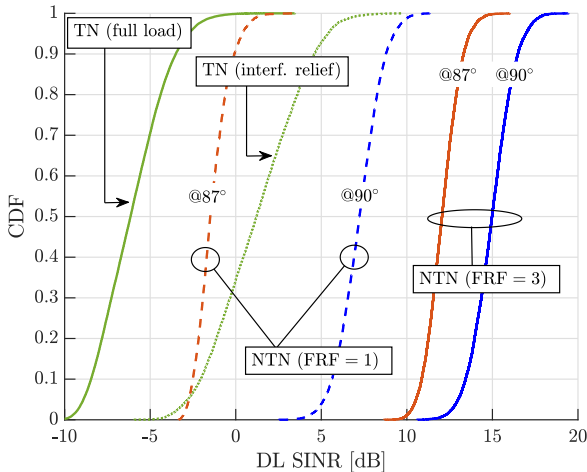


Fig. 2: CDF of the downlink SINR per PRB experienced by UAVs when connected to a standalone TN and when offloaded to a NTN segment. For the latter, two LEO satellite elevation angles and two beam frequency reuse patterns are considered. The SINR experienced from a TN with interference relief is also shown for comparison.

$\min\{B_x/B_k, |\mathcal{U}_x|\}$ users scheduled simultaneously, each for a fraction of time $\eta_k = N_x/|\mathcal{U}_x|$. This choice is owed to the limited power budget available at the user [23].

IV. NUMERICAL RESULTS

In this section, we conduct downlink and uplink experiments to evaluate the performance gains provided by UAV traffic offloading in an integrated TN-NTN. We consider UAVs flying at $h_{\text{UAV}} = 150$ m, which is known to be a challenging scenario for GUE-UAV coexistence [28].

A. Downlink Experiments

Fig. 2 shows the CDF of the downlink SINR per PRB experienced by UAVs when connected to a standalone TN and when offloaded to a NTN segment. For the latter, two LEO satellite elevation angles (90° and 87°) and two beam frequency reuse patterns (FRF = 1 and FRF = 3) are considered.⁴ For comparison, the figure also shows the SINR experienced by UAVs from a TN when the dominant interfering TN cells are turned off to guarantee a minimum SINR of -5 dB (a proxy for coverage [28]). The following observations can be made:

- Standalone TNs struggle to provide reliable coverage to high UAVs, with their SINR falling below -5 dB in 70% of the cases (solid green). This is in line with previous results [1].
- Offloading UAVs to the NTN segment ensures coverage, yielding SINRs ranging between -3 dB and 17 dB depending on the LEO satellite elevation angle and the beam frequency reuse pattern considered, as discussed in what follows.
- Moving from FRF = 3 to FRF = 1 entails full reuse and thus inter-beam interference. The latter degrades the median SINR by approximately 8 dB (solid vs. dashed blue) and 14 dB (solid vs. dashed red) for a LEO satellite at elevation angles of 90° and 87° , respectively.

⁴Note that the downlink SINR does not depend on the UAV penetration.

- The UAV SINR experiences a prominent degradation when the LEO satellite moves from 90° to 87° , due to a larger propagation distance and a lower antenna gain. Indeed, given the HPBW of 4.41° , an elevation angle of 87° implies being served nearly at the edge of a beam. Nonetheless, all NTN-offloaded UAVs still remain in coverage, even in the presence of inter-beam interference (dashed red).
- By design, TN interference relief through cell switch-off guarantees coverage for all UAVs (dotted green). However, the resulting SINRs are lower than those attainable via NTN offloading. Moreover, such approach sacrifices a considerable amount of radio resources, since relieving each UAV of the dominant interference requires approximately 12 TN cells to be idle. The latter results in a capacity loss for legacy GUEs, quantified in the sequel.

Fig. 3 shows the mean and 95%-tile downlink rates achievable by GUEs and UAVs in 3GPP Cases 2 and 3, respectively corresponding to one active UAV every 10 TN cells and one active UAV per TN cell. In this figure, FRF = 3 is assumed, corresponding to higher SINRs on the NTN segment, but also to a reduction of 2/3 of the available bandwidth. The rates computation follows the methodology in (6), assuming users distributed over an urban area $A_U = 52$ km², roughly the size of the city of Barcelona. Fig. 3 considers four different scenarios: (i) a standalone TN serving both GUEs and UAVs; (ii) a standalone TN where dominant interfering cells are switched off on certain PRBs to ensure UAV coverage; (iii) and (iv) an integrated TN-NTN where UAV traffic is offloaded to a LEO satellite seen at 90° and 87° , respectively. Fig. 3 carries the following messages:

- In Case 2—corresponding to 72 active UAVs over the urban area considered—offloading downlink UAV traffic to the NTN segment results in a remarkable five-fold increase in the UAV rates when the LEO satellite is at 90° .
- Owing to a more stable NTN link budget, the rates of NTN-offloaded UAVs exhibit less variance than their TN counterpart, with a small relative gap between mean and 95%-tile rates. In all scenarios considered, the mean UAV rates remain around the recommended 60–100 kbps for C&C [11]. This occurs even in Case 3—corresponding to 720 active UAVs over the urban area—and when the LEO satellite moves from 90° to 87° .
- In a standalone TN, DL rates are independent of the UAV penetration assumed, since the total number of users served by each cell remains unchanged. However, offloading UAVs to the NTN slightly increases the GUE rates, as the capacity of each TN cell has to be shared among fewer users.
- Standalone TNs with interference relief guarantee similar mean rates for the UAVs as the NTN does in Case 2. This however comes at the expense of reducing the legacy GUE rates, a shortcoming that NTN offloading does not entail.

B. Uplink Experiments

Fig. 4 shows the CDF of the uplink SINR per PRB experienced by GUEs and UAVs in Case 3, when all are connected to a standalone TN and when UAV traffic is offloaded to a NTN

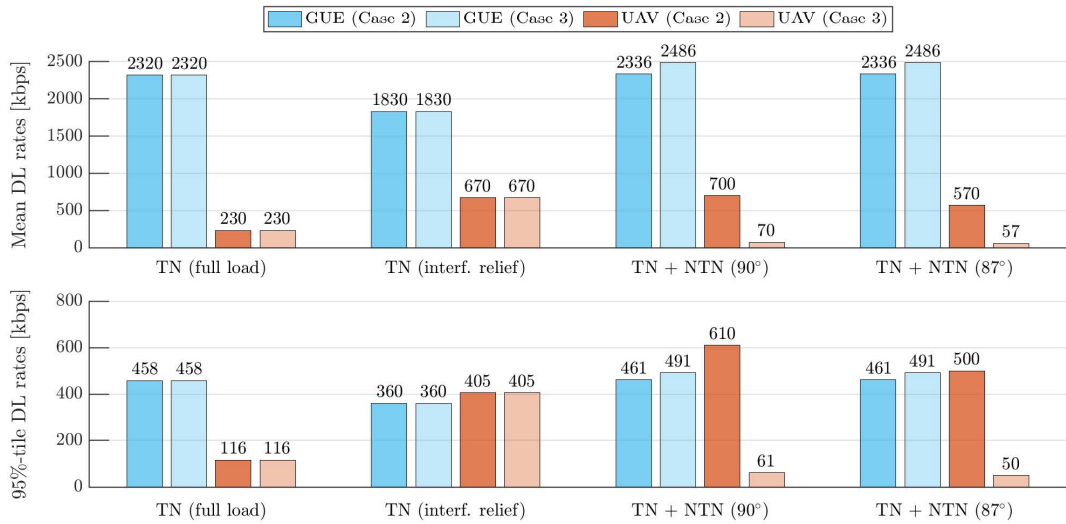


Fig. 3: Mean and 95%-tile downlink rates for GUEs and UAVs when: (i) all are served by a fully loaded TN; (ii) interference relief is guaranteed at UAVs through reserved resources; (iii) and (iv) UAVs are offloaded to a NTN segment at 90° and 87° , respectively, with FRF = 3. Both 3GPP Case 2 and Case 3 are considered, respectively corresponding to a penetration of 72 and 720 UAVs in the urban area.

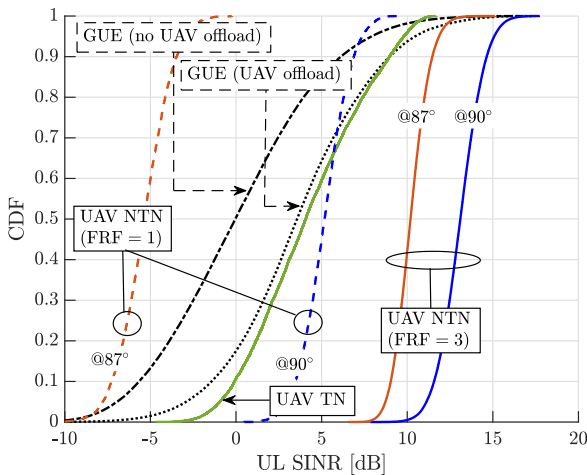


Fig. 4: CDF of the uplink SINR per PRB experienced by GUEs and UAVs in Case 3 when all are connected to a standalone TN and when UAVs are offloaded to a NTN segment. For the latter, two LEO satellite elevation angles and two FRF values are considered.

segment. For the latter, two LEO satellite elevation angles and two beam frequency reuse patterns are considered. The following remarks can be made:

- Even in the presence of fractional power control, the uplink interference generated by UAVs may jeopardize the GUE performance, causing their SINR to drop below -5 dB in 12% of the cases (dash-dotted black).⁵ Such outage is drastically reduced to only 1% by offloading the UAV traffic to the NTN (dotted black).
- When offloaded to the NTN, UAVs see a boost in their uplink SINR as long as the inter-beam interference is kept at bay (solid green vs. blue/red curves). While the median

⁵Assigning and tuning separate power control parameters for GUEs and UAVs may reduce the GUE outage at the expense of the UAV performance.

SINR gain can reach up to 9 dB over the TN baseline in ideal conditions (LEO satellite at 90° and FRF = 3, solid blue), some UAVs may be forced into outage in worse scenarios (LEO satellite at 87° with full frequency reuse, dashed red).

Fig. 5 completes the picture by showing the mean and 95%-tile uplink rates for GUEs and UAVs when: (i) all are served by a fully loaded TN; (ii) the TN employs interference coordination, allocating GUEs and UAVs separate radio resources in a proportion designed to guarantee 100 kbps C&C rates at the UAVs; (iii) and (iv) UAVs are offloaded to a NTN segment at 90° and at 87° , respectively. Again, 3GPP Case 2 and Case 3 are both considered for the penetration of UAV users. Fig. 5 prompts the following important observations:

- In Case 2, a standalone TN is capable of ensuring coverage to most GUEs and UAVs. In Case 3, offloading uplink UAV traffic to the NTN enhances the GUE rates by about 50%, though the latter comes at the expense of reduced UAV rates.
- Even in Case 3—with as many as one active UAV per cell across an urban area the size of Barcelona—and with a bandwidth of only 10 MHz per beam, NTN-offloaded UAVs achieve rates in the order of 60 kbps for C&C.
- NTN-offloading outperforms a standalone TN that enforces time-frequency orthogonality between GUEs and UAVs, since the latter sacrifices a large amount of radio resources, resulting in poor data rates.

V. CONCLUSION

In this paper, we studied supporting UAV communications through an integrated TN-NTN operating below 6 GHz. By offloading UAV traffic to a LEO spaceborne segment, we aimed at guaranteeing reliable UAV C&C coverage without degrading the performance of coexisting GUEs. Our study revealed that NTN-offloaded UAVs flying at 150 m see their downlink outage drastically reduced from 70% to nearly zero. UAVs also experience an uplink SINR boost as long as the

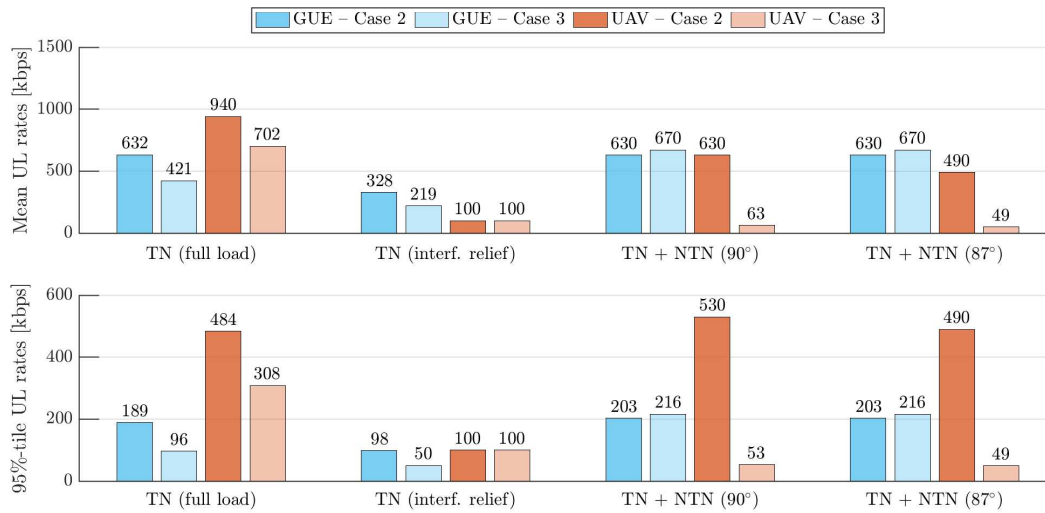


Fig. 5: Mean uplink rates for GUEs and UAVs when: (i) all are served by a fully loaded TN; (ii) a standalone TN reserves radio resources to UAVs to guarantee 100 kbps C&C rates; (iii) UAVs are offloaded to a NTN segment at 90°; and (iv) UAVs are offloaded to a NTN segment at 87°. 3GPP Case 2 and Case 3 are both considered for the UAV density.

LEO satellite constellation is sufficiently dense to guarantee a minimum elevation angle. Offloading UAVs to the NTN may also benefit legacy GUEs, particularly in the uplink as it prevents outages of around 12% that GUEs would otherwise incur. Despite the limited bandwidth available below 6 GHz, NTN-offloaded UAVs meet minimum C&C rate requirements even across an urban area the size of Barcelona with as many as one active UAV per cell. With the lower UAV penetration envisioned in the short-to-medium term, proportionally higher rates can be expected, enabling aerial broadband applications.

REFERENCES

- [1] G. Geraci *et al.*, “What will the future of UAV cellular communications be? A flight from 5G to 6G,” *IEEE Commun. Surveys Tuts.*, pp. 1–1, 2022.
- [2] Y. Zeng, Q. Wu, and R. Zhang, “Accessing from the sky: A tutorial on UAV communications for 5G and beyond,” *Proceedings of the IEEE*, vol. 107, no. 12, pp. 2327–2375, 2019.
- [3] Q. Wu *et al.*, “A comprehensive overview on 5G-and-beyond networks with UAVs: From communications to sensing and intelligence,” *IEEE J. Sel. Areas Commun.*, vol. 39, no. 10, pp. 2912–2945, 2021.
- [4] M. Mozaffari *et al.*, “A tutorial on UAVs for wireless networks: Applications, challenges, and open problems,” *IEEE Commun. Surveys Tuts.*, vol. 21, no. 3, pp. 2334–2360, third quarter 2019.
- [5] J. Buczek, L. Bertizzolo, S. Basagni, and T. Melodia, “What is a wireless UAV? A design blueprint for 6G flying wireless nodes,” in *Proceedings of the 15th ACM Workshop on Wireless Network Testbeds, Experimental Evaluation & Characterization*, 2022, p. 24–30.
- [6] N. Cherif, W. Jaafar, H. Yanikomeroglu, and A. Yongacoglu, “3D aerial highway: The key enabler of the retail industry transformation,” *IEEE Commun. Mag.*, vol. 59, no. 9, pp. 65–71, 2020.
- [7] 3GPP, “TS 22.125. Unmanned Aerial Systems (UAS) Support in 3GPP; Stage 1; Release 17,” 2019.
- [8] Y. Zeng *et al.*, *UAV Communications for 5G and Beyond*. Wiley – IEEE Press, 2020.
- [9] W. Saad, M. Bennis, M. Mozaffari, and X. Lin, *Wireless Communications and Networking for Unmanned Aerial Vehicles*. Cambridge University Press, 2020.
- [10] A. S. Abdalla, K. Powell, V. Marojevic, and G. Geraci, “UAV-assisted attack prevention, detection, and recovery of 5G networks,” *IEEE Wireless Commun.*, vol. 27, no. 4, pp. 40–47, 2020.
- [11] 3GPP Technical Report 36.777, “Study on enhanced LTE support for aerial vehicles (Release 15),” Dec. 2017.
- [12] 3GPP, “RP-212715 New Work Item ID on NR support for UAV,” 2021.
- [13] M. M. U. Chowdhury, I. Guvenc, W. Saad, and A. Bhuyan, “Ensuring reliable connectivity to cellular-connected UAVs with uptilted antennas and interference coordination,” *arXiv:2108.05090*, 2021.
- [14] W. Xia *et al.*, “Generative neural network channel modeling for millimeter-wave UAV communication,” *IEEE Trans. Wireless Commun.*, pp. 1–1, 2022.
- [15] S. Kang *et al.*, “Millimeter-wave UAV coverage in urban environments,” in *Proc. IEEE Globecom*, 2021.
- [16] A. Garcia-Rodriguez *et al.*, “The essential guide to realizing 5G-connected UAVs with massive MIMO,” *IEEE Commun. Mag.*, vol. 57, no. 12, pp. 84–90, 2019.
- [17] C. D’Andrea *et al.*, “Analysis of UAV communications in cell-free massive MIMO systems,” *IEEE Open J. Commun. Society*, vol. 1, pp. 133–147, 2020.
- [18] J. Sedin, L. Feltrin, and X. Lin, “Throughput and capacity evaluation of 5G New Radio non-terrestrial networks with LEO satellites,” in *Proc. IEEE Globecom*, 2020.
- [19] F. Rinaldi *et al.*, “Non-terrestrial networks in 5G & beyond: A survey,” *IEEE Access*, vol. 8, 2020.
- [20] O. Kodheli *et al.*, “Satellite communications in the new space era: A survey and future challenges,” *IEEE Commun. Surveys Tuts.*, vol. 23, no. 1, pp. 70–109, 2021.
- [21] M. Giordani and M. Zorzi, “Non-terrestrial networks in the 6G era: Challenges and opportunities,” *IEEE Network*, vol. 35, no. 2, pp. 244–251, 2021.
- [22] G. Geraci, D. López-Pérez, M. Benzaghta, and S. Chatzinotas, “Integrating terrestrial and non-terrestrial networks: 3D opportunities and challenges,” *arXiv:2207.10385*, 2022.
- [23] 3GPP Technical Report 38.821, “Solutions for NR to support non-terrestrial networks (NTN) (Release 16),” Dec. 2019.
- [24] 3GPP Technical Report 38.811, “Study on New Radio (NR) to support non-terrestrial networks (Release 15),” Sep. 2020.
- [25] 3GPP Technical Report 38.901, “Study on channel model for frequencies from 0.5 to 100 GHz (Release 16),” Dec. 2019.
- [26] M. M. Azari, G. Geraci, A. Garcia-Rodriguez, and S. Pollin, “UAV-to-UAV communications in cellular networks,” *IEEE Trans. Wireless Commun.*, vol. 19, no. 9, pp. 6130–6144, 2020.
- [27] P. Baracca *et al.*, “Downlink performance of uplink fractional power control in 5G massive MIMO systems,” in *Proc. IEEE Globecom*, 2018.
- [28] G. Geraci *et al.*, “Understanding UAV cellular communications: From existing networks to massive MIMO,” *IEEE Access*, vol. 6, 2018.